Vol. 21, No. 3(2022) IA2892
Revista Mexicana de Ingeniería Química

Influence of initial copper concentration, pH, and cross-linked alginate-chitosan and alginate-chitosan-*Aspergillus australensis* composite beads on the adsorption capacity and removal efficiency of copper ions

Influencia de la concentración inicial de cobre, pH y perlas compuestas reticuladas de alginato-quitosano y alginato-quitosano-*Aspergillus australensis* en la capacidad de adsorción y eficiencia de remoción de iones de cobre

F.A. Dávila-Parra[1], M. Plasencia-Jatomea[2], O. Monge-Amaya[1], A.R. Mártin-García[1], J. de la Vega-Olivas[1], F.J. Almendariz-Tapia[1]*

[1]*Departamento de Ingeniería Química y Metalurgia, Universidad de Sonora, Rosales y Blvd. Luis Encinas, Hermosillo, Sonora, México, C.P. 83000.*

[2]*Departamento de Investigación y Posgrado en Alimentos, Universidad de Sonora, Rosales y Blvd. Luis Encinas, Hermosillo, Sonora, México, C.P. 83000.*

Received: July 20, 2022; Accepted: November 16, 2022

Abstract

Copper (Cu) is a toxic heavy metal whose concentration must be reduced to values under the environmental standard before discharges can be released into the environment. Due to its characteristics, using different adsorbents for biosorption is a convenient method for removing heavy metals. Alginate and chitosan are biopolymers that have shown high potential as adsorbents. This investigation discusses the influence of pH, initial concentration of copper (Co), and the type of immobilized bead in the adsorption capacity and removal efficiency of copper from synthetic solutions. FT-IR analysis showed cross-linked composite beads of alginate-chitosan (ICB) and alginate-chitosan-*Aspergillus australensis* (IBB) possess different functional groups. The analysis made with the kinetic models showed that the adsorption mechanism was governed by diffusion through interface and chemical adsorption. Adsorption capacity depends on pH and Co. Maximum average adsorption capacity was 4.46 mg/g at 600 mg/L and pH 4.5 for ICB. Statistical analysis demonstrated that Co, pH, and their interactions significantly affect removal efficiency. Besides, the highest removal efficiency was 36.18% ± 1.87 at pH 4.5, 150 mg/L for IBB. These biomaterials could be a potential adsorbent for removing copper from wastewater.

Keywords: copper, chitosan, alginate, cross-linked composite beads, adsorption.

Resumen

El cobre (Cu) es un metal pesado tóxico. Su concentración debe reducirse por debajo de las normas ambientales antes de descargarse al medio ambiente. La biosorción utiliza diferentes adsorbentes y es un método efectivo para remoción de metales pesados. Quitosano y alginato son biopolímeros que han mostrado alto potencial adsorbente. En este trabajo se estudió la influencia de la concentración inicial de cobre (Co), pH y tipo de perla inmovilizada sobre la capacidad de adsorción y eficiencia de remoción de cobre. El análisis FT-IR de perlas compuestas reticuladas de alginato-quitosano (ICB) y alginato-quitosano-*Aspergillus australensis* (IBB) mostró diferentes grupos funcionales. El análisis de los modelos cinéticos mostró que el mecanismo de adsorción se rige por difusión y adsorción química. La capacidad de adsorción media máxima fue de 4.46 mg/g a 600 mg/L y pH 4.5 para ICB, y se observó que depende del pH y de Co. El análisis estadístico demostró que Co, pH y sus interacciones poseen efectos significativos en la eficiencia de remoción, la cual fue de 36.18% ± 1.87 a pH 4.5 y 150 mg/L para IBB. Estos biomateriales podrían ser unos adsorbentes potenciales para la remoción de cobre de aguas residuales.

Palabras clave: cobre, quitosano, alginato, perlas compuestas reticuladas, adsorción.

* *Corresponding author. E-mail*: javier.almendariz@unison.mx

https://doi.org/10.24275/rmiq/IA2892
ISSN:1665-2738, *issn-e*: 2395-8472

1 Introduction

Heavy metals have been found to be one of the main wastewater contaminants in industrial, mining, and agricultural. Therefore, the concentration of these heavy metals must be reduced to values under the standard concentration established by the government before discharges can be released into the environment (Upadhyay *et al*., 2021) as the indiscriminate discharge of heavy metals directly affects human health and the natural ecosystem. Copper, according to environmental standards, must be eliminated from aqueous environments since it is considered a highly toxic heavy metal (Khademian *et al*., 2020). In México, the NOM-001-SEMARNAT-1996, allows a maximum copper concentration of 4 mg/L for wastewater discharge to soils or rivers, while the NOM-127-SSA1-1994 allows a maximum copper concentration of 2 mg/L for water intended for use, and human consumption (SEMARNAT, 1994, 1996). Some sources that allow the entrance of copper into the environment are copper polishing, mining, painting, plating, and printing operations (Ayangbenro & Babalola, 2017). Although copper is necessary for humans, as well as for plants, animals, and microorganisms, prolonged exposure may produce adverse effects. Contaminated food and beverages or inhalation are entry pathways of human copper ingestion. High levels of copper in humans have been found to cause liver cirrhosis, anemia, brain and kidney damage, stomach and intestinal irritation, and even death (National Institutes of Health, 2019). On the other hand, plants and microorganisms can cause chlorosis, retard growth and oxidative stress, disrupt cellular function and inhibit enzyme activities (Ayangbenro & Babalola, 2017). High concentrations of soluble copper salts in animals can cause the development of intravascular hemolysis, liver failure, and renal failure (Bayón Sanz, 2015; Londoño Franco *et al*., 2016; Rodríguez Heredia, 2017). Due to their characteristics (bioaccumulation, biotransformation, high toxicity), heavy metals are considered environmentally toxic (Rodríguez Heredia, 2017). Some accidents involving mine tailing spills of acidic solutions with heavy metals concentrations above environmental standards have occurred recently. The presence of high copper concentration (114 mg/L) was found in the chemical composition of acidic ferro-cupriferrous solution spilled from the mining operation of Cananea, Sonora (Romero-Lázaro *et al*., 2019). In an acid mine drainage characterization from the Tiza mine a copper concentration of 12 mg/L was found (Cervantes Macedo, 2014). Groundwater from a mining community in the North of México was collected for characterization, and a concentration of copper of 210 mg/L was found (Alcázar-Medina *et al*., 2020). Therefore, it is necessary to design technologies that contribute to the removal of high heavy metal concentrations from mining spills and thus avoid the impact of these contaminants on the ecosystem. A broad range of technologies designed to remove heavy metals from wastewater do so by altering the chemical structure of pollutants and thus be able to isolate or destroy them through reverse osmosis, chemical precipitation, solvent extraction, and membrane processes. However, these methods often cause secondary pollution and are expensive (Upadhyay *et al*., 2021). Adsorption of wastewater heavy metals is a removal technique that has drawn attention, due to its minimum costs, effectiveness, and simplicity. Minimum secondary pollution is produced when biological materials are used during adsorption, therefore, the biosorption term can be used to describe the passive adsorption of toxic substances into biological materials. Due to its characteristics, biosorption using a combination of adsorbents is one of the best methods for the treatment of wastewater contaminated with heavy metals, such as copper. As a result, researchers have been interested in the development of effective, biodegradable, and inexpensive adsorbents (Emenike *et al*., 2022; Upadhyay *et al*., 2021). Adsorbents that are simple in use, effective, and abundant in the natural environment are an attractive alternative to traditional adsorbents. Biosorption can be conducted through immobilization using natural organic material. This class of biomaterials includes chitosan, alginate, cellulose, charcoal, straw, plant fibers, seaweeds (Asencios *et al*., 2022), corncob (Tejeda-Tovar *et al*., 2021), rice, etc. Both chitosan and alginate are known as biopolymers carriers. Carrier biomaterials should possess characteristics such as being non-toxic to the environment, insoluble, easily accessible, inexpensive, stable, and can be regenerated for future cycles of use (Dzionek *et al*., 2016; Velkova *et al*., 2018). Chitosan is a biopolymer obtained from the deacetylation of chitin. It owns the advantage that its source material is a biopolymer highly abundant in nature, which is extricated from the exoskeleton of sea crustacean shells and insects and has shown significant potential as an adsorbent. Alginate is another biopolymer used for the removal of heavy metals from wastewater.

This biopolymer is isolated from brown macroalgae and is applied as an adsorbent and as an ionic exchanger. Biomass obtained from microorganisms such as bacteria, fungi, and yeasts can also be used as an adsorbent. Fungal biomass can be employed as a biosorbent due to the presence, in the cell wall, of a vast range of functional groups that are involved in the biosorption of metallic ions (Bennett *et al*., 2013; Dhankhar & Hooda, 2011; Dziwulska *et al*., 2004). The mycromycetes of the genera *Aspergillus*, *Rhizopus*, *Trichoderma*, etc., are the most used as free and immobilized fungal biomass (Dhankhar & Hooda, 2011) The mycromycetes can rapidly grow on inexpensive culture media, and the amount of biomass produced is abundant. It is worth pointing out that fungal biomass is naturally abundant in the environment and can be found in contaminated sites (Bennett *et al*., 2013; Velkova *et al*., 2018). Contreras-Cortés *et al*., isolated native metal-tolerant fungi from heavy metal-contaminated sediments corresponding to *Aspergillus australensis*. Copper tolerance tests and adsorption studies were performed using the live and inactive fungi biomass immobilized on textiles. *Aspergillus australensis* has been shown to be metal-tolerant fungi because the highest radial growth reached was at 250 and 500 ppm of $CuSO_4$ (Contreras-Cortés *et al*., 2020). Soil microorganisms possess a high tolerance to heavy metals. These organisms have acquired this characteristic through evolutionary adaptation to contaminated environments. Tolerance to heavy metals in microorganisms such as fungi involves specific and non-specific mechanisms such as metal binding to cell walls and extracellular and intracellular sequestration (Nouha *et al*., 2016). Studies have reported that copper is an essential part of the metabolism of microorganisms, as it actively participates in several metabolic functions (X. Liu *et al*., 2020; Stern, 2010). In addition, the presence of chitin in the cell wall of *Aspergillus australensis* was found by fluorescence microscopy after exposure to 50 and 250 ppm of copper (Contreras-Cortés *et al*., 2020). This polysaccharide is a metal-binding site (Vendruscolo *et al*., 2017). The adaptability shown by the fungi is related to a gene responsible for synthesizing the metallothionein protein, which is responsible for binding different transition metals. This protein has been postulated to be responsible for detoxifying some heavy metals in distinct species of microorganisms. Metallothionein proteins can bind Ni, Zn, Cd, Pb, and Cu with affinities that depend upon the bioavailability and concentration of heavy metals (Parameswari *et al*., 2021). Concerning adsorption studies, copper removal efficiency and adsorption capacity of live fungi biomass immobilized on the textile was 40.26 ± 3.32% and 2.65 ± 0.21 mg/g at pH 5.0 and 40°C, respectively, while with the inactive fungi biomass immobilized on the textile the highest copper removal efficiency and adsorption capacity was 34.46% and 2.46 ± 0.303 mg/g at pH 5.5 and 35°C, respectively (Contreras-Cortés *et al*., 2020). Using inactive biomass brings some advantages, such as working in a wide range of pH values. It also contributes to the implementation of an economical process due to the elimination of the use of nutrient culture media and the maintenance of pure microbial cultures, which implies low costs and the use of simple equipment. However, the use of materials that support the inactive biomass is recommended due to the small particle size, the difficult separation between the solid-liquid phase, and low mechanical stability. Therefore fungal biomass is a material that can be combined with adsorbent materials to enhance heavy metal removal (Bennett *et al*., 2013; Cañizares-Villanueva, 2000; Varnam & Evans, 2000; Vijayaraghavan & Yun, 2008). On the other hand, a broad range of immobilization techniques is available. Ionotropic gelation allows the production of composite beads by electrostatic interactions between two ionic biopolymers with oppositely charged ions to initiate a cross-linking process (Ahirrao *et al*., 2013; Dzionek *et al*., 2016; Pedroso-Santana & Fleitas-Salazar, 2020), moreover microbial cells can be part of the immobilization process. Mokale *et al*., 2014 synthesized chitosan-alginate gel beads by ionotropic gelation with a physical cross-linking. The beads were prepared by dropping an alginate solution into a chitosan solution. As a result, the beads presented an alginate core and a chitosan skin. During this process, the chitosan amino groups protonate and the alginate carboxylic acid groups are ionized. Calcium chloride-chitosan solution was used for sodium alginate gelation to improve the stability of the chitosan-alginate bead gel. It has been found that the presence of calcium ions in chitosan solution had the potential to bind chitosan into the gel bead (Mokale *et al*., 2014). Researchers have studied copper removal from synthetic solutions using different biomaterials matrices as adsorbents. Initial copper concentration, pH, biosorbent type (biomaterial and biomass), and immobilization technique have been evaluated to explain the adsorbent yield as enlisted in Table 1.

Table 1. Performance on different biopolymers with immobilized microorganism cells as biosorbents for adsorption capacity and copper removal from synthetic solutions at different initial condition.

Carrier	IM	IT	$[Cu]_o$ (mg/L)	pH	AT (min)	Temperature (°C)	Adsorption capacity (mg/g)	Removal efficiency (%)	Reference
Sodium alginate-Chitosan	—-	Cross-linking	100	2-9	120	25	4.22	81	(Kuczajowska-Zadrozna *et al.*, 2020)
Sodium alginate-Chitosan	*Aspergillus australensis*	Cross-linking	176	5	1440	35	26.1	23.22 ± 0.37	(Contreras-Cortés *et al.*, 2019)
Sodium alginate	*Penicillium citrinum*	Entrapment	20	2	60	32	2.9-3.1	70-75	(Verma *et al.*, 2013)
Chitosan	*Bacillus subtilis*	Entrapment	50	3	1440	37	—-	40-45	(Liu *et al.*, 2013)
Sodium alginate	*Trichoderma asperellum*	Cross-linking	100	2	480	28 ± 2	10-20	—-	(Tan and Ting, 2012)
Alginate-Gelatin-PVA	*Bacillus CR-7*	Cross-linking	50	4.5	90	35	20-30	30-35	(Xu *et al.*, 2011)

IM: Immobilized microorganism; IT: Immobilization technique; $[Cu]_o$: Initial copper concentration; AT: Adsorption time.

Therefore, by introducing immobilized cells into biomaterials, several mechanisms can contribute to the biosorption of wastewater contaminants (Dzionek *et al.*, 2016). To implement a way to contribute to the removal of metallic ions from wastewater, we developed cross-linked composite beads of alginate-chitosan and alginate-chitosan-*Aspergillus australensis*. This investigation discusses the influence of factors such as the initial concentration of copper, pH, and the type of immobilized bead in the capacity of adsorption and removal efficiency of ionic copper from synthetic solutions. We also evaluated three kinetic models to enhance the understanding of the adsorption process mechanism.

2 Materials and methods

2.1 Copper synthetic solutions

A 1000 mg/L stock solution of copper (Cu^{+2}) was prepared by dissolving copper sulfate ($CuSO_4 \cdot 5H_2O$) (7758-99-8, J. T. Baker, Estado de México, México) in triple distilled water, and it was further diluted to the initial concentrations of 150 and 600 mg/L.

2.2 Production of inactivated Aspergillus australensis biomass

Inactivated *Aspergillus australensis* biomass was grown on a semisynthetic Czapek broth medium enriched with yeast extract. The semisynthetic medium was prepared using the following composition: 1 g/L K_2HPO_4 (7758-11-4, Fermont, Nuevo León, México); 3 g/L $NaNO_3$ (7631-99-4, Meyer, Ciudad de México, México); 0.5 g/L $MgSO_4$ (10034-99-8, Faga Lab, Sinaloa, México); 0.5 g/L KCl (7447-40-7, Faga Lab, Sinaloa, México); 0.01 g/L $FeSO_4 \cdot 7H_2O$ (7782-63-7, Faga Lab, Sinaloa, México); 30 g/L saccharose (57-50-1, J. T. Baker, Estado de México, México) and 5 g/L yeast extract (S071004, SOLBIOSA, Jalisco, México), also $CuSO_4 \cdot 5H_2O$ was added until reached a 10 mg/L concentration. A suspension of 5×10^5 spores/mL was inoculated in 100 mL of Czapek broth and grown in conical flasks incubated in an orbital shaker (CVP-500, Scientific) at 30°C, 150 rpm for 7 days. The inactivated fungal biomass (IB) was obtained by autoclave sterilization (STME, Market Forge) at 121°C for 20 min, and then it was dried for 24 h at 60°C. Once dried, the biomass was milled and sieved up to 180 μm mesh size until a powder was obtained.

2.3 Sodium alginate gel preparation

A sodium alginate solution (SA) (9005-38-3, Meyer, Ciudad de México, México) was prepared to dissolve 1 g in 100 mL of triple distilled water at 60 - 70°C and stirred until its dissolution (Contreras-Cortés *et al.*, 2019).

2.4 Chitosan gel preparation

The solution of chitosan of medium molecular weight (CMMW) (9012-76-4, Sigma-Aldrich, Missouri, USA) was prepared by dissolving 2 g in 100 mL of acetic acid (5% v/v) (64-19-7, J. T. Baker, Estado

de México, México) and stirring until its dissolution (Contreras-Cortés *et al*., 2019).

2.5 *Synthesis of composite and biocomposite beads*

The synthesis of alginate-chitosan (composite) and alginate-chitosan-*Aspergillus australensis* biomass composite beads (biocomposite) was accomplished in two steps. Step 1: SA solution was prepared at 1%(w/v), then the solution was homogenized for 30 min. For biocomposites, 0.1 g of IB was added. Step 2: CMMW was prepared at 2%(w/v) with acetic acid and mixed in a beaker with 85 mL of $CaCl_2$ at 3%(w/v) (10043-52-4, Fermont, Nuevo León, México) and the solution was homogenized for 15 min. The SA and SA-IB solution was dripped using a peristaltic pump into the solution prepared in step 2 (CMMW + $CaCl_2$) to precipitate and form the composite and biocomposite beads.

2.6 *Characterization of composite and biocomposite beads*

2.6.1 *Diameter size and adsorbents composition*

The diameter size of the composite (ICB) and biocomposite (IBB) beads was measured with ImageJ software (v. 1.53e). Diameter size was considered as the average of 10 individual composite beads measured vertically and horizontally.

2.6.2 *Fourier-Transform Infrared Spectroscopy (FT-IR)*

The functional groups present on ICB and IBB adsorbent beads, pure CMMW, SA, and IB were determined with the Fourier Transform Infrared Spectroscopy analysis (FT-IR) (Nicolet iS50, Thermo Scientific). The attenuated total reflection (ATR) accessory was used. Measurements were performed with 128 average scans in a spectral range of 4000-400 cm^{-1}. The spectra of pure CMMW, AS, and raw biomass was performed in powder form. Also, ICB (CMMW + AS) and IBB (CMMW + AS + IB) were analyzed in powder form to interpret the interactions between materials.

2.7 *Batch adsorption tests using ICB and IBB*

Adsorption experiments were performed using ICB and IBB in wet form. First, ICB and IBB adsorbent beads were gently blotted using absorbent paper and weighed, then a total of 0.3 g of both adsorbent beads were placed in serological bottles with 10 mL of a copper solution containing 150 and 600 mg/L of initial copper concentration (Co) at two pH values (2.5 and 4.5). The serological bottles were placed in an orbital incubator at 30°C and 150 rpm. Samples of 0.1 mL were taken at 20, 60, 120, 180, 360, and 720 min. Liquid phase samples were analyzed by ion-exchange chromatography (IC) (881 Compact IC pro, Metrohm) to determine the copper concentration. The experiment was conducted in triplicate. The following equation was used to determine the copper adsorption over time q_t (mg/g) (Eq. 1):

$$q_t = \frac{(C_o - C_t)V}{m} \tag{1}$$

where: q_t = mass of copper (Cu) adsorbed per mass of ICB or IBB (mg/g), Co = initial copper concentration (mg/L), C_t = copper concentration after contact time, t (mg/L), m = adsorbent (ICB or IBB) weight (g), and V = solution copper volume (L).

Copper ion removal efficiency (%R) was calculated with the equation (Eq. 2):

$$\%R = \frac{C_o - C_t}{C_o} \times 100 \tag{2}$$

where Co = initial copper concentration (mg/L), C_t = copper concentration after contact time, t (mg/L).

The data of the adsorption kinetics obtained were correlated to pseudo-first-order (PFO), pseudo-second-order (PSO), and Elovich kinetic models. The kinetic model characteristic parameters, which represent the adsorption ion copper dynamic on the immobilized beads were obtained using a Microsoft Excel solver (v. 2205) by a non-linear regression optimization technique employing the sum of the squared error function (SSE) (Eq. 3) as minimization criteria (Pinzón-Bedoya & Villamizar, 2009).

$$SSE = \sum_{i=1}^{n} (Y_{obs,i} - Y_{pred,i})^2 \tag{3}$$

2.7.1 *Pseudo-first-order model (PFO)*

The PFO model is commonly related to the initial stage of adsorption. The adsorption kinetic follows this model when the adsorbate diffusion occurs through the adsorbent interface. The model assumes that the rate of change concerning time in adsorbate adsorption is proportional to the difference between the amount of adsorbate uptake at equilibrium and the amount of adsorbate uptake with time (Sahoo & Prelot, 2020).

The nonlinearized form of the PFO model is presented in the following equation (Eq. 4):

$$q_t = q_e(1 - e^{-k_1 t}) \tag{4}$$

where q_e and q_t are the adsorption capacity in the equilibrium, and after contact time t, respectively (mg/g), and k_1 is the adsorption rate constant of the PFO model (min^{-1}).

2.7.2 *Pseudo-second-order model (PSO)*

The PSO model predicts the performance over the entire adsorption process. The adsorption rate depends on the adsorption capacity and not on the adsorbate concentration. This model presumed that the rate-limiting step is chemical adsorption (chemisorption). The advantage over the PFO model is that the model itself permits the calculation of the equilibrium adsorption capacity. Thus, there is no requirement to obtain the adsorption capacity at equilibrium from an experiment (Sahoo & Prelot, 2020).

The nonlinearized form of the PSO model is presented in the following equation (Eq. 5):

$$q_t = \frac{k_2 q_e^2 t}{1 + k_2 q_e t} \tag{5}$$

where q_e is the adsorbed copper amount at equilibrium (mg/g), and k_2 is the rate constant of the PSO model (g/mg min).

2.7.3 *Elovich model*

In the Elovich kinetic model, there is the assumption of an energetically heterogeneous adsorbent surface, and a chemisorption phenomenon occurs on the surface. At low surface coverage, neither desorption nor adsorbate interactions could affect the adsorption kinetics (Ferreira *et al*., 2019; Sahoo & Prelot, 2020). The non-linear form of the model is obtained with the equation (Eq. 6):

$$q_t = \frac{1}{\beta} \ln(\beta \alpha t) \tag{6}$$

where α (mg/g min) is the initial adsorption rate, and β (g/mg) is the desorption constant.

2.8 *Model evaluation indices for copper adsorption*

Three indices were evaluated to find which kinetic model best describes the behavior of the experimental data: the coefficient of determination (R^2), the IA index (IA), and the root mean square error (RMSE) (Alavi & Ansari, 2022; McCuen *et al*., 2006; Rahman & Sathasivam, 2015; Suteu *et al*., 2016).

The IA index (Eq. 7) varies between 0 and 1. Where 1 indicates the accordance between the predicted and the observed values. Values of 0 indicate no agreement at all.

The R^2 coefficient (Eq. 8), which ranges from 0 to 1 explains the goodness of fit that exists between the observed and predicted values. A higher R^2 coefficient indicates a closer linear relationship between observed and predicted values.

The RMSE (Eq. 9) is always a non-negative value ranging from 0 to ∞. The nearer RSME is to 0, the better the observed values fit the model equation.

$$IA = 1 - \frac{\sum_{i=1}^{n}(Y_{obs,i} - Y_{pred,i})^2}{\sum_{i=1}^{n}(|Y_{obs,i} - \overline{Y}_{obs}| + |Y_{pred,i} - \overline{Y}_{obs}|)^2} \tag{7}$$

$$R^2 = \left[\frac{\sum_{i=1}^{n}(Y_{pred,i} - \overline{Y}_{pred})(Y_{obs,i} - \overline{Y}_{obs})}{\sqrt{\sum_{i=1}^{n}(Y_{pred,i} - \overline{Y}_{pred})^2 \sum_{i=1}^{n}(Y_{obs,i} - \overline{Y}_{obs})^2}} \right]^2 \tag{8}$$

$$RMSE = \sqrt{\frac{1}{n}\sum_{i=1}^{n}(Y_{obs,i} - Y_{pred,i})^2} \tag{9}$$

2.9 *Statistical analysis for copper removal efficiency*

A 2^3 factorial design (three factors at two levels) was employed to evaluate the interactions between pH, initial concentration of copper (mg/L) (Co), and the immobilized bead type (IBT). The extreme levels (high and low) represented by +1 and -1 are listed in Table 2. An array was created according to their extreme levels, 8 experiments were performed in a random order to avoid systematic errors. The experiment was conducted in triplicate. Analysis of variance (ANOVA) was performed to elucidate the main effects and interactions between factors. The response variable was the copper removal efficiency (%R). The removal efficiency data reported were the mean values of three replicates. The results were analyzed with RStudio (v. 4.2.0), and all the analyses were carried out with a significance level of $\rho \leq 0.05$.

Table 2. Initial concentration, pH and immobilized bead type as factors and their high and low levels studied in the 2^3 experimental design.

Factors	**Levels**	
	Low level (-1)	High level (+1)
Initial concentration (Co)	150	600
pH	2.5	4.5
Immobilized bead type (IBT)	ICB	IBB

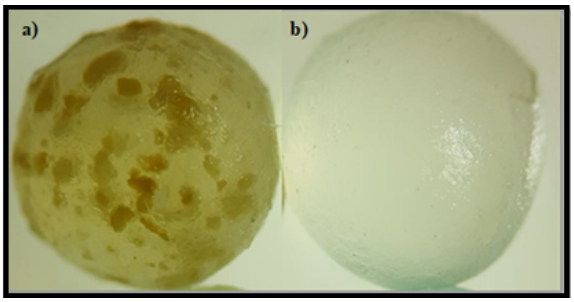

Figure 1. Physical appearance of cross-linked composite beads with and without immobilized fungal biomass before adsorption experiments are as follows: a) IBB and b) ICB.

The mathematical model of a 2^3 factorial experimental design is presented (Eq. 10):

$$\hat{y} = \beta_0 + \beta_1 IBT + \beta_2 C_o + \beta_3 pH + \beta_{12} IBT C_o + \beta_{13} IBT\, pH + \beta_{23} C_o pH + \beta_{123} IBT C_o pH \quad (10)$$

Where IBT is the coded variable representing the immobilized bead type (ICB or IBB), Co is the initial concentration of copper, and pH is the pH of the copper solution. The β_i signs are the coefficients obtained from the regression model, and $\hat{y}$ is the predicted response.

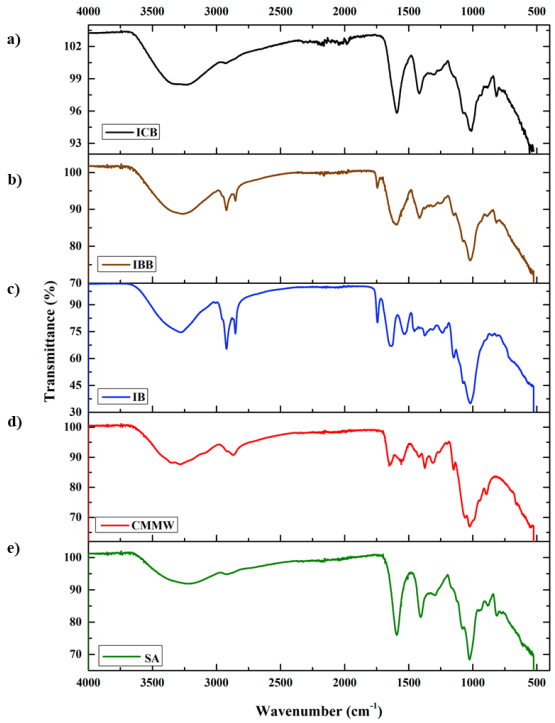

Figure 2. FT-IR spectra of cross-linked composite beads with and without immobilized fungal biomass are as follows: a) ICB; b) IBB; c) IB, d) CMMW; e) SA.

3 Results and discussions

3.1 *Synthesis and characterization of ICB and IBB*

The appearance of IBB (Figure 1a) was opaque brown because of immobilized biomass, while ICB (Figure 1b) was an opaque white color. Both bead types were firm to the touch. The average diameter size for IBB and ICB was 2.95 ± 0.04 mm and 2.77 ± 0.03 mm, respectively. The bigger diameter size of IBB, compared with ICB, does seem to depend on immobilized biomass. This result ties well with previous studies wherein adsorbents beads (alginate-chitosan-*Aspergillus australensis*) diameter average size obtained was 2.0 ± 0.1 mm. These similar adsorbent beads have been used in an adsorption copper ions study (Contreras-Cortés *et al.*, 2019). According to the synthesis procedure, the mass fraction composition of the beads was 96.9% water, 3.0% calcium alginate, and 0.1% QMPM for ICB and 97.2% water, 2.2% calcium alginate, 0.6% fungal biomass, and 0.1% QMPM for IBB, both in wet basis. Wet beads have around 90%-95% of water content, which confirms the nature of the hydrogels

(Zazzali *et al*., 2019). On the other hand, at different polymerization times, alginate beads have around 78%-86% of water content (Block, 2003).

The FT-IR spectra of SA, CMMW, and IB in the wavenumber region of 4000 cm^{-1}-500 cm^{-1} are illustrated in Figure 2. As shown in Figure 2e the spectra for SA present the band 3208 cm^{-1} which are attached to OH groups stretching. The band 1593 cm^{-1} depicts asymmetric stretching of the -COOH group. In the region of 1405-1024 cm^{-1}, stretching of COO- groups are observed. The peak of 809 cm^{-1} represents the mannuronic acid residues (Contreras Cortés, 2019; Lawrie *et al*., 2007; Papageorgiou *et al*., 2010; Torres *et al*., 2016). In Figure 2d, the spectra of CMMW are presented. The band 3282 cm^{-1} represents the vibration of primary NH_2 groups and OH groups associated with the pyranose ring. The peaks of 1653 and 1558 cm^{-1} represent vibration associated with amide I and amine II, respectively. The band 1149 cm^{-1} represents the amine group and the band 1024 cm^{-1} is attributed to the COC-bond extension, indicating the saccharide structure indicates on the chitosan (Ibitoye *et al*., 2018; Kuczajowska-Zadrozna *et al*., 2020). In Figure 2c the IB spectra are presented. The band 3280 cm^{-1} is associated with protein content (primary amide groups). The spectra between 2950 cm^{-1} to 2800 cm^{-1} denoted the region of phospholipids, while the peak of 1744 cm^{-1} is related to carboxylic groups, both present in the fungal cell wall. The bands 1637 cm^{-1} and 1533 cm^{-1} are attached to the protein and peptides content of *Aspergillus*, specifically, amide I and amide II, respectively, whereas the peaks of 1455 cm^{-1} and 1236 cm^{-1} are attached to polysaccharides and lipids content of the fungi, specifically amide III. The bands present in the region of 1200-900 cm^{-1} (1149 cm^{-1} and 1020 cm^{-1}) are associated with phospholipids, nucleic acid, the carbohydrates cell wall of fungi, and cell wall polysaccharides (García Hernández, 2017; Saif *et al*., 2021). In Figures 2a and 2b, the ICB and IBB spectra are presented, respectively. The spectra for IBB (Fig. 2b) present the peaks associated with the stretching of COO- groups related to SA, functional groups associated with protein, peptides, phospholipid content of fungi and carboxylic groups of *Aspergillus* fungi. The spectra for ICB (Fig. 2a) present the peaks related to mannuronic acid residues and OH groups related to SA, and the saccharide chitosan structure. As can be seen, no chitosan representative peaks appear in the IBB spectra, while in the ICB spectra, one representative band of saccharide chitosan structure is found. As can be expected, no peaks associated with fungal biomass appeared in the ICB spectra. Moreover, it can be observed less intense bands of carboxylate groups related to sodium alginate in IBB and ICB spectra because of the interaction with divalent calcium ions to form calcium alginate gel (Nastaj *et al*., 2016).

3.2 Adsorption kinetic studies using ICB and IBB

The adsorption performance of ICB and IBB adsorbents under different conditions was investigated to elucidate the adsorption mechanism. The adjustment of the non-linear equations of the three kinetic models to the experimental adsorption data is shown in Figure 3. The evaluation indices values, SSE error function, R^2, IA, and RMSE have been used as a criterion to assess the correlation between the experimental data and the model-predicted values. Indices values and the parameters of the kinetic models are presented in Table 3. The non-linear fitting of the three kinetics models at Co = 150 mg/L and pH 2.5 and 4.5, for both ICB and IBB adsorbents beads are shown in Figures 3a and 3b. According to Table 3, the experimental kinetic data for ICB and IBB at pH 2.5 (Fig. 3a) fitted more accurately with the PFO model in agreement with lower values of SSE (0.0015 and 0.0466) and RMSE (0.0159 and 0.0763), which means an improved fitting of experimental data with the kinetic model, otherwise with higher values of R^2 (0.9990 and 0.9693) and IA (0.9997 and 0.9922) evaluation indices, which means the experimental data were well matched with PFO model. Calculated $q_{e,cal}$ (1.3511 mg/g and 1.2310 mg/g) values from PFO model agree well with the experimental $q_{e,exp}$ (1.3594 mg/g and 1.2186 mg/g) values for both adsorbents. On the other hand, at Co = 150 mg/L and pH 4.5 (Fig. 3b), experimental values for IBB adsorbent were best described by the PFO model because the values of SSE (0.0371), RMSE (0.0681), R^2 (0.9866) and IA (0.9966). The experimental data for ICB adsorbent showed the best fitting to PSO model (SSE = 0.0360; RMSE= 0.0718; R^2= 0.9821; IA= 0.9555) (Fig. 3b). This suggests that the PFO mechanism is predominant for ICB only at pH 2.5 and IBB for both pHs tested. Therefore, the external and internal diffusion through the interface may be the rate-limiting step controlling the adsorption processes, which also means that a few active sites exist in both ICB and IBB adsorbents beads at the conditions described above.

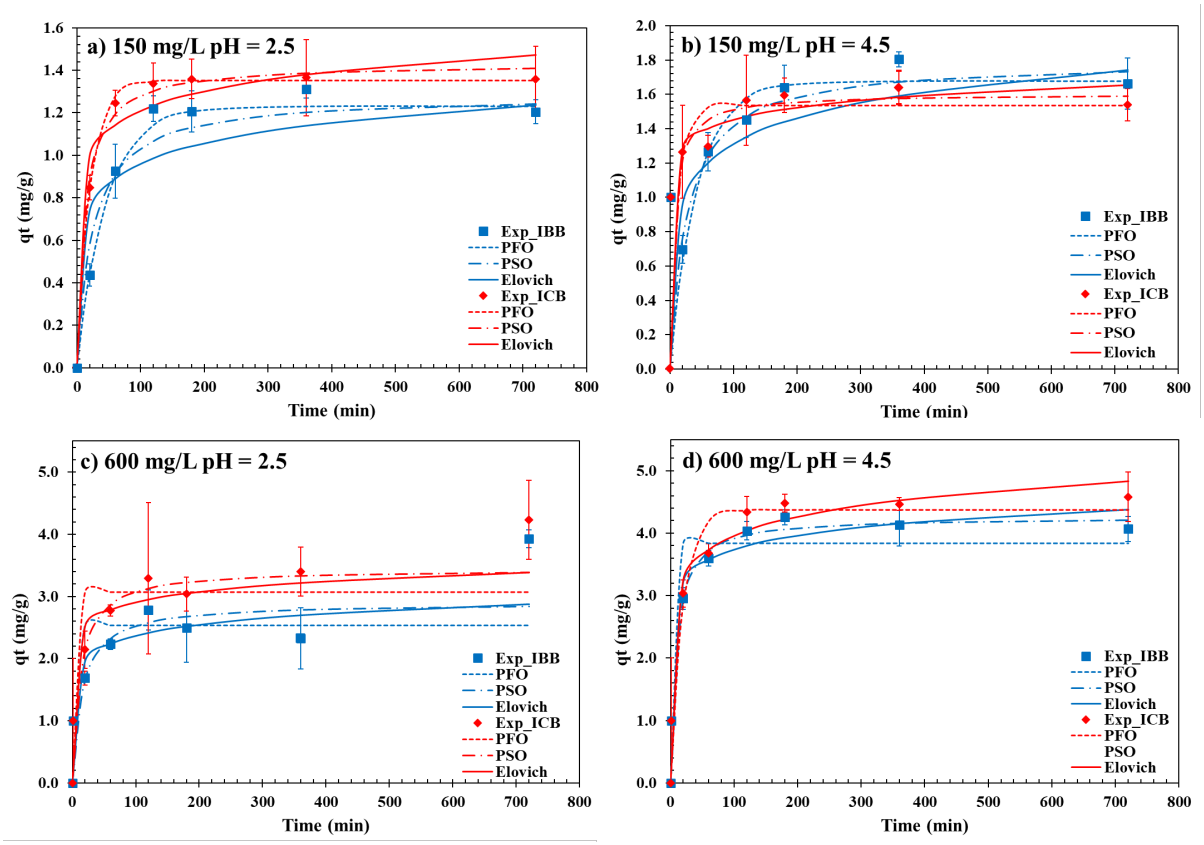

Figure 3. Fitted kinetic curves for the adsorption of copper ions on cross-linked composite beads with (IBB) and without (ICB) immobilized fungal biomass at a) 150 mg/L, pH 2.5; b) 150 mg/L, pH 4.5; c) 600 mg/L, pH 2.5; d) 600 mg/L, pH 4.5 (V = 10 mL, m_{ICB} = 0.3 g, m_{IBB} = 0.3 g, 150 rpm, 30°C).

The rate-limiting step that controls the adsorption process for ICB at pH 4.5 does seem to depend on chemical adsorption, which is a PSO mechanism. It implies plentiful active sites on the ICB surface adsorbent beads when the pH changes from 2.5 to 4.5. Interactions as ion exchange and electrostatic attractions between copper ions and active sites could be considered onto ICB surface adsorbent beads (Nastaj *et al*., 2016; Sahoo & Prelot, 2020; Wang & Guo, 2020). Also, at Co = 600 mg/L and pH 2.5 and 4.5 for both ICB and IBB adsorbents beads, the calculated parameters are shown in Table 3. The non-linear fitting of the three kinetic models at the conditions described above is presented in Figures 3c and 3d. As can be seen, for pH 2.5 and ICB adsorbent, (Fig. 3c) and pH 4.5 (Fig. 3d) for both ICB and IBB adsorbents, experimental kinetic data fitted more accurately to the PSO model since the lower values of SSE (0.5305, 0.0789 and 0.0768) and RMSE (0.3357, 0.1824 and 0.118). It means the best fitting between experimental data and the kinetic model, moreover higher values of R^2 (0.9410, 0.9914 and 0.9943) and IA (0.9797, 0.9962 and 0.9985) indicate a closer linear relation and almost a perfect agreement, respectively, between experimental data and predicted values, comparing with the PFO and Elovich model evaluation indices and error function values. As a result, there is a definitive agreement between calculated $q_{e,cal}$ (3.7930 mg/g, 4.6542 mg/g, and 4.2605 mg/g) values and experimental $q_{e,exp}$ (3.4003 mg/g, 4.4819 mg/g and 4.1353 mg/g) for PSO model comparing with PFO and Elovich models. All of this implies that the limiting step that controls the process of adsorption is chemisorption (Wang & Guo, 2020), implicating that either electron exchange or valence forces through sharing between ICB and IBB with copper are occur (Samuel *et al*., 2013). The non-linear fitting for IBB adsorbent at Co = 600 mg/L and pH 2.5 is shown in Figure 3c.

Table 3. Parameters of fitted kinetic models for the adsorption of copper ions on cross-linked composite beads with (IBB) and without (ICB) immobilized fungal biomass at different initial copper concentrations and pH values.

	ICB		IBB		ICB		IBB	
pH	**2.5**				**4.5**			
Initial concentration (mg/L)	**150**	**600**	**150**	**600**	**150**	**600**	**150**	**600**
PFO								
k_1 (min^{-1})	0.048	41.305	0.0219	11.9963	0.0802	0.0526	0.0234	23.9525
$q_{e,cal}$ (mg/g)	1.3511	3.1452	1.231	2.5751	1.5337	4.377	1.6756	3.8423
$q_{e,exp}$ (mg/g)	1.3594	3.4003	1.2186	2.3258	1.5389	4.4819	1.6633	4.1353
SSE	0.0015	2.4192	0.0466	2.8413	0.0673	0.355	0.0371	1.1911
R^2	0.999	0.778	0.9693	0.6667	0.9665	0.9773	0.9866	0.914
IA	0.9997	0.9325	0.9922	0.8897	0.9508	0.9932	0.9966	0.9774
RMSE	0.0159	0.5923	0.0763	0.6384	0.0987	0.2457	0.0681	0.3923
PSO								
k_2 (g/min mg)	0.0575	0.0139	0.0317	0.0138	0.0984	0.0187	0.0207	0.0264
$q_{e,cal}$ (mg/g)	1.4318	3.793	1.2839	3.1877	1.6026	4.6542	1.796	4.2605
$q_{e,exp}$ (mg/g)	1.3594	3.4003	1.2186	2.3258	1.5389	4.4819	1.6633	4.1353
SSE	0.0092	0.5305	0.1076	1.3132	0.036	0.0789	0.0451	0.0768
R^2	0.994	0.941	0.929	0.8376	0.9821	0.9914	0.9834	0.9943
IA	0.9985	0.9797	0.9806	0.9478	0.9955	0.9962	0.9957	0.9985
RMSE	0.0367	0.3357	0.116	0.4581	0.0718	0.1824	0.075	0.1118
Elovich								
β (g/mg)	7.4988	1.9182	7.1438	2.0439	9.7665	2.2593	4.5784	4.1823
α (mg/g min)	11.6076	1.5753	1.3205	0.6805	1461.8515	33.755	0.8842	13484.2871
$q_{e,cal}$ (mg/g)	1.473	4.0066	0.9844	3.3808	1.6532	4.8305	1.7425	4.3798
$q_{e,exp}$ (mg/g)	1.3594	3.4003	1.2186	2.3258	1.5389	4.4819	1.6633	4.1353
SSE	0.0611	0.221	0.2832	0.9334	0.0431	0.2731	0.2323	0.3315
R^2	0.9571	0.9313	0.8116	0.8513	0.9775	0.9606	0.914	0.9722
IA	0.9882	0.9734	0.9451	0.9463	0.9941	0.987	0.977	0.9923
RMSE	0.0993	0.3765	0.1881	0.4557	0.0813	0.3329	0.1704	0.2484

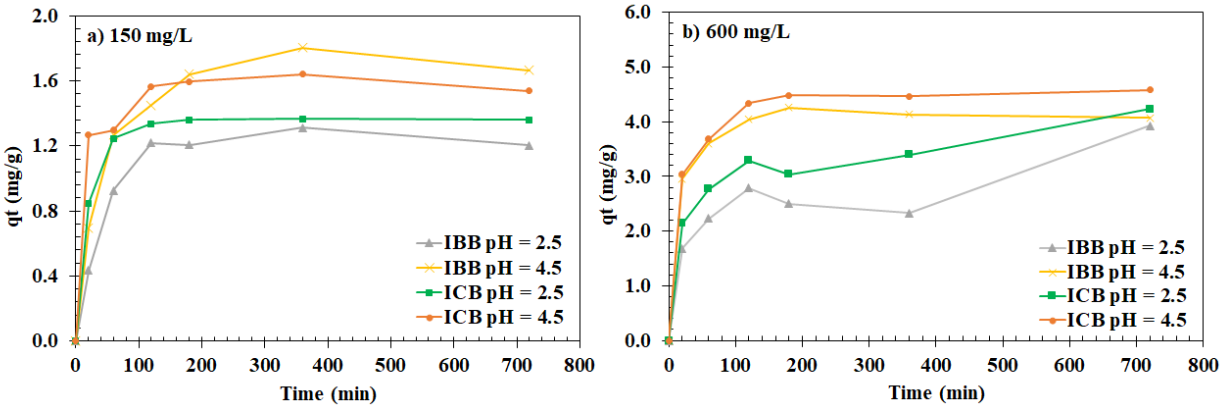

Figure 4. Effect of pH on the adsorption of copper ions onto cross-linked composite beads with (IBB) and without (ICB) immobilized fungal biomass at a) 150 mg/L, and b) 600 mg/L (V = 10 mL, m_{ICB} = 0.3 g, m_{IBB} = 0.3 g, 150 rpm, 30°C)

According to the low values of SSE (0.9334) and RMSE (0.4557) and higher values of R^2 (0.8513) and IA (0.8463) from Table 3, it can be observed the Elovich model best explains the adsorption mechanism of copper on IBB adsorbent. This result implies that the IBB adsorbent surface is energetically heterogeneous, and also chemical adsorption is implicated in the adsorption process (Ferreira *et al*., 2019; Guo *et al*., 2022; Sahoo & Prelot, 2020). García-González *et al*., reported the use of chitosan-cellulose (Q-C) cryogel as an adsorbent for the removal of copper from aqueous solutions. PSO and Elovich kinetic models best described the adsorption process, indicating a heterogeneous adsorbent surface and a chemisorption process (García-González *et al*., 2016).

3.3 Effect of pH on copper kinetic adsorption

The initial pH effect on the adsorption of copper by both ICB and IBB adsorbent beads after 720 minutes is depicted in Figure 4. Initial copper concentrations of 150 (Fig. 4a) and 600 mg/L (Fig 4b) at both pH values (2.5 and 4.5) at 30°C and 150 rpm were studied. The curve shown in Figure 4a gives the adsorption capacity of both adsorbent beads depending on the time at the pHs evaluated. As a result, when pH incremented from 2.5 to 4.5 adsorption capacity of both adsorbent beads increased until it almost reached a steady state. As can be seen in Figure 4b, at Co = 600 mg/L same behavior occurred when pH increased from 2.5 to 4.5 for both adsorbent beads. The adsorption capacity through the time for ICB and IBB adsorbent beads at pH 4.5 was almost constant from 180 minutes until 720 minutes. The final pH values at 150 mg/L and pH 2.5 for ICB and IBB were 2.80 and 2.84, respectively, while at 600 mg/L were 2.70 and 2.69, respectively. On the other hand, at pH 4.5, the copper solution final pH at 150 mg/L for ICB and IBB were 3.94 and 3.76, respectively, while at 600 mg/L were 3.99 and 3.76, respectively. Furthermore, due to the final pH values, the protonation/deprotonation of the functional adsorbent groups could have happened. The final pH value increased during the adsorption process at initial acidic conditions (pH 2.5), due to the protonation of active sites attendant on the surface of the adsorbents as carboxylate group (COO^-), present in the calcium alginate and phosphate group (PO_4^{3-}) present in the fungal cell wall. Consequently, the lower adsorption capacity value obtained for both ICB and IBB at pH 2.5 at 150 and 600 mg/L compared to pH 4.5 could be related to electrostatic repulsive forces between copper ions present in the solution and the protonated active spaces on the adsorbent surface (Nurak *et al*., 2012; Tan & Ting, 2012). On the other hand, at an initial pH value of 4.5, the final pH values of the copper solution decrease during the adsorption process at 150 and 600 mg/L for ICB and IBB, because of the deprotonation of the carboxylic group (-COOH) of the mannuronic acid residues present in calcium alginate. Therefore, the hydrogen ion concentration is higher in the copper solution (Xu *et al*., 2011). As a result, the carboxylic group acts as a cation exchanger (Ca^{+2} is exchanged for Cu^{+2}), and attractive forces between the carboxylate (COO-) adsorbent surface group and the copper ions solution (Cu^{+2}) may occur. Therefore, under this condition, the adsorption capacity of the adsorbents increases (An *et al*., 2013; Fotsing *et al*., 2020; Lawrie *et al*., 2007; Xu *et al*., 2011). Heavy metal adsorption onto adsorbents is highly dependent on the pH solution (Nastaj *et al*., 2016). The values of pH possess influence over the active sites of the adsorbents and their surface charge. The metal species solubility could be modified due to the pH solution (Emenike *et al*., 2022). Notably, the analysis of the results of copper ion adsorption exhibited adsorption capacity over time of both adsorbents beads was influenced by the studied pH values in both initial copper concentrations (150 and 600 mg/L), and the adsorption capacity was favored by increasing the pH of the copper solution from 2.5 to 4.5. However, after the adsorption process at 150 and 600 mg/L, both at pH 2.5, a mass fraction of ICB (40.9% and 13.4%) and IBB (15.7% and 0.6%) adsorbent beads was dissolved because of this acidic condition. Tan & Ting studied copper adsorption by alginate beads with immobilized *Trichoderma asperellum* cells. Different pH values were evaluated during the adsorption process. The least copper adsorption was at pH 2 for alginate beads and alginate beads with immobilized cells. This suggests that the adsorption capacity depends on the protonation/deprotonation of the carboxyl groups present in alginate and fungal cell walls (Tan & Ting, 2012).

3.4 Effect of initial copper concentration on copper kinetic adsorption

Initial copper concentration was adjusted at 150 and 600 mg/L for adsorption study onto ICB and IBB adsorbents beads with pH 4.5 at 30°C for 720 minutes. The adsorption capacity for both adsorbents beads depending on the time at the two initial copper concentration values is illustrated in Figure 5.

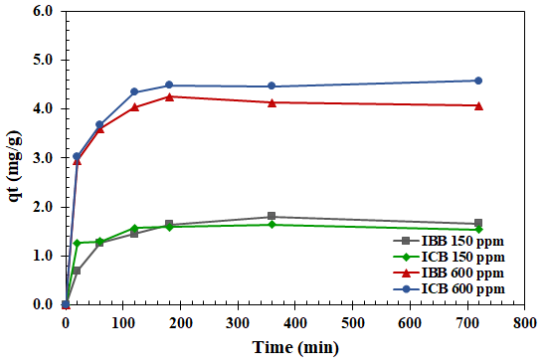

Figure 5. Effect of the initial copper concentration on the copper ions adsorption onto cross-linked composite beads with (IBB) and without (ICB) immobilized fungal biomass (V = 10 mL, m_{ICB} = 0.3 g, m_{IBB} = 0.3 g, 150 rpm, 30°C).

As a result, when the concentration of copper increased from 150 mg/L to 600 mg/L, the adsorption capacity through time for both ICB and IBB adsorbents beads increased. For the first 120 minutes, a sudden increase in adsorption capacity for both adsorbents beads occurred, but then a steady-state appeared until 720 minutes. From 120 to 720 minutes, the average adsorption capacity accomplished for ICB and IBB adsorbents beads was 1.5846 mg/g and 1.6396 mg/g, respectively, at Co = 150 mg/L, while at Co = 600 mg/L, the average adsorption capacity for ICB and IBB adsorbents beads was 4.4664 mg/g and 4.1245 mg/g, respectively. For both adsorbent bead types, the adsorption at Co = 600 mg/L was always higher than at Co = 150 mg/L. This result suggests that higher copper concentrations increased the mass transfer driving force between aqueous solution and adsorbent beads. Also, the number of copper ions adsorbed onto the adsorbent beads increased. Moreover, the initial metal ion concentration is dependent on the available active sites on the adsorbent surface (Emenike *et al*., 2022; Y. Liu *et al*., 2013). Emenike *et al*., studied copper adsorption on TiO_2 NPs and reported that increasing the concentration of copper ion increase the adsorption capacities of the nano adsorbents. Besides, they pointed out that this behavior is a tendency in most adsorption studies (Emenike *et al*., 2022). Torres-Cabán *et al*., evaluated the adsorption capacity of copper using sodium alginate beads. The adsorption capacity was 17.83 mg/g, which agrees with Yu *et al*., who evaluated the adsorption capacity of copper from sodium alginate microparticles, the reported adsorption capacity was 18.32 mg/g. The latter study also reports an adsorption capacity of 4.24 mg/g with chitosan nanoparticle beads crosslinked with sodium tripolyphosphate. However, the amino groups of the synthesized adsorbent of pure chitosan tend to protonate if exposed to acidic pH media, which originates a partial or total dissolution of the chitosan beads (Sánchez-Duarte *et al*., 2017; Torres-Caban *et al*., 2019; Yu *et al*., 2013).

3.5 *Influence of initial copper concentration, pH, and immobilized bead type in copper removal efficiency*

The significant factors and their interactions in the regression model can be determined from the analysis of variation (ANOVA), which is shown in Table 4. Because of the F-ratio values and ρ-values < 0.05, the most important effect is Co, followed by pH, and finally, the interaction between Co and pH since they significantly affect copper removal efficiency. On the other hand, some main effects and their interactions can be discarded since these do not offer any statistical significance over the response (ρ-value > 0.05).

Table 4. Analysis of variance of the 2^3 factorial design at different initial concentrations, pH values and adsorbent bead type.

Source of variance	DF	SS	MS	F-ratio	ρ-value
Immobilized bead type (IBT)	1	8.9	8.9	1.621	0.2211
Initial concentration (Co)	1	502.1	502.1	91.501	<0.0001*
pH	1	125.9	125.9	22.937	0.0002*
IBT x Co	1	3.2	3.2	0.579	0.4578
IBT x pH	1	9	9	1.638	0.2188
Co x pH	1	66.3	66.3	12.08	0.0031*
Error	16				

* Significant factor ($\alpha \leq 0.05$); DF: degrees of freedom; SS: sum of squares; MS: mean square

Table 5. Experimental design matrix: coded and actual values for the experimental design and experimental and predicted copper removal efficiency values as the response.

	Coded values			Actual values			Response	
							Copper removal efficiency (%R)	
Run	**Co**	**pH**	**IBT**	**Co**	**pH**	**IBT**	**Observed**	**Predicted**
1	-1	-1	-1	150	2.5	ICB	28.77 ± 1.89	28.7689
2	1	-1	-1	600	2.5	ICB	22.00 ± 1.91	22.0056
3	-1	1	-1	150	4.5	ICB	33.78 ± 1.21	33.7785
4	1	1	-1	600	4.5	ICB	23.70 ± 1.18	23.7078
5	-1	-1	1	150	2.5	IBB	25.38 ± 0.68	28.7689
6	1	-1	1	600	2.5	IBB	20.50 ± 0.44	22.0056
7	-1	1	1	150	4.5	IBB	36.18 ± 1.87	33.7785
8	1	1	1	600	4.5	IBB	21.31 ± 0.61	23.7078

Values represents the average of three replicates ± their standard error.

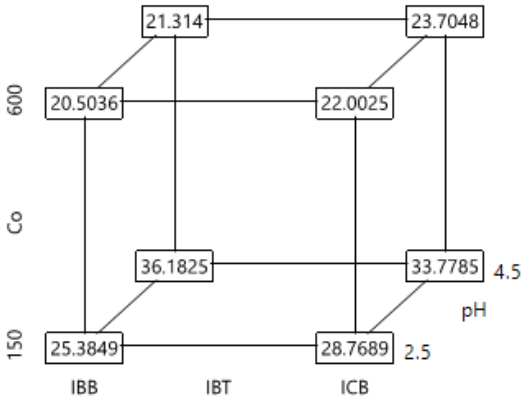

Figure 6. Cube plot for copper removal efficiency at different initial copper concentrations (150 mg/l and 600 mg/l) and pH values (2.5 and 4.5).

From the above ANOVA, the final empirical model (Eq. 11) includes statistically significant main effects and interactions for predicted removal copper efficiency values.

$$\hat{y} = 28.7689 - 6.7632Co + 5.0096pH - 3.3074CopH \quad (11)$$

From Table 5, the higher removal efficiency of copper ions took place at run 7, where the combination of factors such as lower initial concentration, higher pH value, and IBB adsorbent were applied. This may be because the availability of binding sites is higher at 150 mg/L compared to 600 mg/L, therefore leading to more copper ions adsorbed onto the adsorbent surface. Besides, increasing the solution pH value also increments the negative charge on the adsorbent surface, improving the interaction between active sites such as hydroxyl and carboxyl groups and metal cations such as copper (Y. Liu *et al*., 2013).

Based on the correlation between the factors studied and the response obtained, a cube plot was drawn (Fig. 6). It can be seen the highest efficiency of copper removal is achieved using IBB adsorbent beads at 150 mg/L and pH of 4.5. However, when the pH solution value decreases from 4.5 to 2.5, the removal copper efficiency decreases from 36.18% ± 1.87 to 25.38% ± 0.68. Furthermore, the lowest removal copper efficiency was obtained using IBB adsorbent beads at 600 mg/L and a pH of 2.5. This appears to be a case of electrostatic repulsion forces between copper ions and the adsorbent surface since the adsorbent surface is positively charged due to protonation at low pH values, hence the number of binding sites for copper ion adsorption is reduced (Kumararaja *et al*., 2018).

3.5.1 Interaction effects plot

Figure 7 shows the interaction effects between copper removal efficiency and the studied factors. As can be seen, parallel lines are observed for the interaction of the Co and IBT, indicating that there is no significant interaction between both factors. In this interaction, almost a horizontal line at 600 mg/L can be observed, indicating no significant differences in removal copper efficiency among ICB and IBB. A similar trend was observed in the interaction at 600 mg/L and both pH values (4.5 and 2.5). However, evaluating the rate constant between both adsorbent beads at the pH values evaluated, the IBB rate constant showed a higher value than the ICB rate constant, indicating that the adsorption process was faster with IBB adsorbent beads (k_2 = 0.0264 g/mg min).

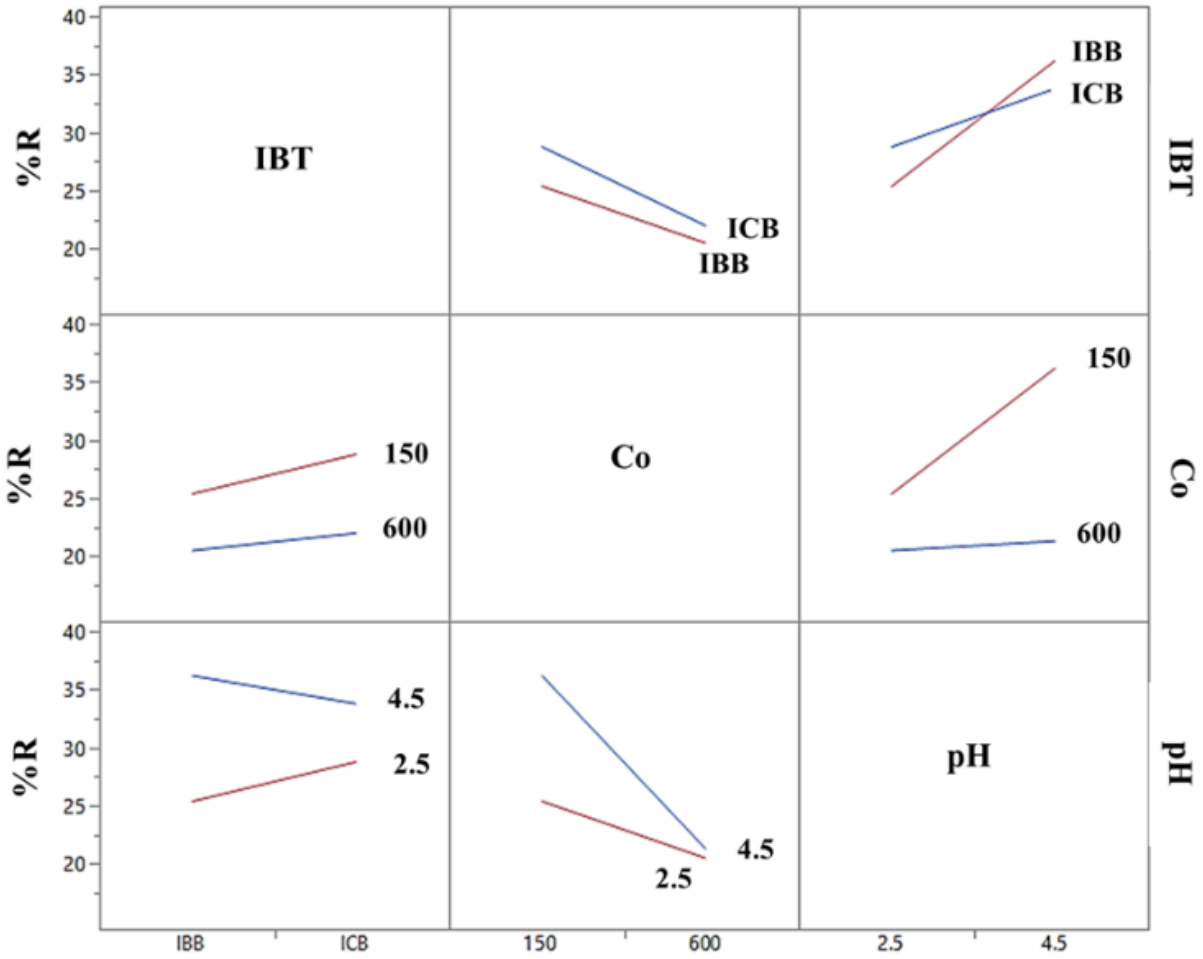

Figure 7. Interaction effects plot for copper removal efficiency at different initial copper concentrations (150 mg/l and 600 mg/l) and pH values (2.5 and 4.5).

Besides, an important effect in the interaction between Co and IBT along with pH and IBT in the highest level of Co and pH can be observed. In these interactions, the highest efficiency of copper removal was achieved at pH 4.5 for both adsorbent beads. On the other hand, the lowest copper removal efficiency was obtained at 150 mg/L for ICB and IBB. When increases the pH value from 2.5 to 4.5 at 150 mg/L a positive effect was observed in the removal of copper efficiency, however at 600 mg/L narrowly increases. On the other hand, while increasing Co from 150 mg/L to 600 mg/L the copper removal efficiency decreases at both pH levels and IBT levels.

Conclusions

FT-IR analysis showed that cross-linked composite beads of alginate-chitosan and alginate-chitosan-*Aspergillus australensis* possess different functional groups because of the biomass content. Also, a bigger diameter size was observed in adsorbent beads with immobilized biomass. Three kinetic models were used to analyze experimental data (PFO, PSO, and Elovich). In most cases, PFO kinetic model best describes experimental data at an initial concentration of copper (150 mg/L), while PSO kinetic model achieved the best fit at 600 mg/L. However, Elovich kinetic model accomplished the highest fit at 600

mg/L, pH 2.5 with IBB adsorbent beads. Hence, the adsorption mechanism is believed to be governed by external and internal diffusion through the interface (PFO) and chemical adsorption (PSO and Elovich). The experiments exhibited that adsorption capacity depends on the pH solution and initial concentration of copper. A maximum average adsorption capacity of 4.46 mg/g at 600 mg/L and pH 4.5 was obtained for ICB adsorbent beads. The 2^3 factorial experimental design was used to determine the pH effect, initial concentration of copper, and immobilized bead type. The statistical analysis demonstrated that the initial concentration of copper, pH, and the interaction between the initial concentration of copper and pH possess significant effects on the copper removal efficiency. The highest removal copper efficiency was 36.18% ± 1.87 at pH 4.5 and Co = 150 mg/L using IBB adsorbent beads. These two adsorbent beads show great promise for copper ion removal at high copper concentrations in acidic conditions. These two parameters can be manipulated to accomplish maximum adsorption capacity and copper removal.

Acknowledgments

The authors would like to thank the Consejo Nacional de Ciencia y Tecnología (CONACyT) and Universidad de Sonora (UNISON) for the scholarship provided to the first author.

Nomenclature

q_t	adsorption capacity of the ICB and IBB absorbents at time t (mg/g)
$q_{e,cal}$	equilibrium adsorption capacity calculated with kinetic models (mg/g)
$q_{e,exp}$	equilibrium experimental adsorption capacity (mg/g)
q_e	equilibrium adsorption capacity (mg/g)
k_1	adsorption rate constant of the PFO kinetic model (min^{-1})
k_2	adsorption rate constant of the PSO kinetic model (g/mg min)
C_o	initial concentration of copper (mg/L)
C_t	concentration of copper after contact time, t (mg/L)
$Y_{obs,i}$	experimental adsorption data (mg/g)
$Y_{pred,i}$	predicted adsorption with the kinetic models (mg/g)
m	adsorbent beads weight (g)
V	volume of the copper solution (L)
%R	copper ion removal efficiency (%)
SSE	sum of the squared error function
R^2	coefficient of determination
RMSE	root mean square error
PFO	pseudo-first-order kinetic model
PSO	pseudo-second-order kinetic model
IB	inactivated fungal biomass
IBB	biocomposite beads
ICB	composite beads
IBT	immobilized bead type
SA	sodium alginate
CMMW	chitosan of medium molecular weight
FT-IR	Fourier Transform Infrared Spectroscopy
IC	ion exchange chromatography
ANOVA	analysis of variance
α	initial adsorption rate (mg/g min)
β	desorption constant (g/mg)
β_i	coefficients of the experimental design model
$\hat{y}$	values of the predicted response

References

Ahirrao, S. P., Gide, P. S., Shrivastav, B., & Sharma, P. (2013). Ionotropic Gelation: A Promising Cross Linking Technique for Hydrogels. *Research and Reviews: Journal of Pharmaceutical and Nanotechnology* 2(1), 1-6.

Alavi, J., & Ansari, S. (2022). Kinetic models evaluation for chemical organic matter removal prediction in a full-scale primary facultative pond treating municipal wastewater. *Water Science and Technology*, 1-16. https://doi.org/10.2166/wst.2022.074

Alcázar-Medina, F. A., Núñez-Núñez, C. M., Villanueva-Fierro, I., Antileo, C., & Proal-Nájera, J. B. (2020). Removal of heavy metals present in groundwater from a northern Mexico mining community using Agave tequilana Weber extracts. *Revista Mexicana de Ingeniería Química 19*(3), 1187-1199. https://doi.org/10.24275/rmiq/Bio1047

An, B., Son, H., Chung, J., Choi, J. W., Lee, S. H., & Hong, S. W. (2013). Calcium and hydrogen effects during sorption of copper onto an alginate-based ion exchanger: Batch and fixed-bed column studies. *Chemical Engineering Journal 232*, 51-58. https://doi.org/10.1016/j.cej.2013.07.079

Asencios, Y. J. O., Parreira, L. M., Perpetuo, E, A., & Rotta, A. L. (2022). Characterization of seaweeds collected from Baixada Santista litoral, and their potential uses as biosorbents of heavy metal cations. *Revista Mexicana de Ingeniería Química 21*(1), 1-22. https://doi.org/10.24275/rmiq/IA2600

Ayangbenro, A. S., & Babalola, O. O. (2017). A new strategy for heavy metal polluted environments: A review of microbial biosorbents. *International Journal of Environmental Research and Public Health 14*(94), 1-16. https://doi.org/10.3390/ijerph14010094

Bayón Sanz, S. (2015). Aplicación de la fitorremediación a suelos contaminados por metales pesados. Tesis de Licenciatura en Edafología, Universidad Complutense, España.

Bennett, R. M., Cordero, P. R. F., Bautista, G. S., & Dedeles, G. R. (2013). Reduction of hexavalent chromium using fungi and bacteria isolated from contaminated soil and water samples. *Chemistry and Ecology 29*(4), 320-328. https://doi.org/10.1080/02757540.2013.770478

Block, W. (2003). Water status and thermal analysis of alginate beads used in cryopreservation of plant germplasm. *Cryobiology 47*(1), 59-72. https://doi.org/10.1016/S0011-2240(03)00069-5

Cañizares-Villanueva, R. O. (2000). Biosorción de metales pesados mediante el uso de biomasa microbiana. *Revista Latinoamericana de Microbiologia 42*(3), 131-143. https://doi.org/10.1016/j.procbio.2004.02.024

Cervantes Macedo, A. H. (2014). Caracterización del drenaje ácido y de las rocas asociadas a una mina para evaluar su posible aplicación en un sistema de tratamiento pasivo. Tesis de Licenciatura en ingeniería de Minas y Metalurgista, Universidad Nacional Autónoma de México, México.

Contreras-Cortés, A. G., Almendariz-Tapia, F. J., Cortez-Rocha, M. O., Burgos-Hernández, A., Rosas-Burgos, E. C., Rodríguez-Félix, F., Gómez-Álvarez, A., Quevedo-López, M. Á., & Plascencia-Jatomea, M. (2020). Biosorption of copper by immobilized biomass of *Aspergillus australensis*. Effect of metal on the viability, cellular components, polyhydroxyalkanoates production, and oxidative stress. *Environmental Science and Pollution Research*. https://doi.org/10.1007/s11356-020-07747-y

Contreras-Cortés, A. G., Almendariz-Tapia, F. J., Gómez-Álvarez, A., Burgos-Hernández, A., Luque-Alcaraz, A. G., Rodríguez-Félix, F., Quevedo-López, M. Á., & Plascencia-Jatomea, M. (2019). Toxicological assessment of cross-linked beads of chitosan-alginate and *Aspergillus australensis* biomass, with efficiency as biosorbent for copper removal. *Polymers 11*(222), 1-17. https://doi.org/10.3390/polym11020222

Contreras Cortés, A. G. (2019). Uso de Biocompositos de Quitosano, Alginato y Biomasa de *Aspergillus australensis* con Aplicación Potencial para Bioeliminar Cobre en Aguas de Uso Agrícola. Universidad de Sonora.

Dhankhar, R., & Hooda, A. (2011). Fungal biosorption-an alternative to meet the challenges of heavy metal pollution in aqueous solutions. *Environmental Technology 32*(5), 467-491. https://doi.org/10.1080/09593330.2011.572922

Dzionek, A., Wojcieszyńska, D., & Guzik, U. (2016). Natural carriers in bioremediation: A review. *Electronic Journal of Biotechnology 23*, 28-36. https://doi.org/10.1016/j.ejbt.2016.07.003

Dziwulska, U., Bajguz, A., & Godlewska-Zyłkiewicz, B. (2004). The Use of Algae *Chlorella vulgaris* Immobilized on Cellex-T Support for Separation/Preconcentration of Trace Amounts of Platinum and Palladium before GFAAS Determination. *Analytical Letters 37*(10), 2189-2203. https://doi.org/10.1081/AL-200026696

Emenike, E. C., Adeniyi, A. G., Omuku, P. E., Okwu, K. C., & Iwuozor, K. O. (2022). Recent advances in nano-adsorbents for the sequestration of copper from water. *Journal of Water Process Engineering 47*, 102715. https://doi.org/10.1016/j.jwpe.2022.102715

Ferreira, S. A., Mota, A. A., Oliveira, M. A., Rodrigues, I. L. F., Pacífico, N. S., da Silva, E.

J., Abagaro, T. O. B., Saraiva, D. G., de Castro, J. R. A., Teixeira, N. P. R., & Sousa Neto, O. V. (2019). Equilibrium and Kinetic Modelling of Adsorption: Evaluating the Performance of an Adsorbent in Softening Water for Irrigation and Animal Consumption. *Revista Virtual de Química 11*(6), 1752-1766. https://doi.org/10.21577/1984-6835.20190123

Fotsing, P. N., Woumfo, E. D., Măicăneanu, S. A., Vieillard, J., Tcheka, C., Ngueagni, P. T., & Siéwé, J. M. (2020). Removal of Cu(II) from aqueous solution using a composite made from cocoa cortex and sodium alginate. *Environmental Science and Pollution Research 27*(8), 8451-8466. https://doi.org/10.1007/s11356-019-07206-3

García-González, R., Gómez-Espinosa, R. M., Ávila-Pérez, P., Garcia-Gaitán, B., García-Rivas, J. L., & Zavala-Arce, R. E. (2016). Estudio de biosorción de Cu^{2+} en el criogel quitosano-celulosa. *Revista Mexicana de Ingeniería Química 15*(2), 311-322.

García Hernández, M. de L. Á. (2017). Obtención de cepas fúngicas metalófilas autóctonas de México para su aplicación en tecnologías sustentables. Tesis de Doctorado en Ciencias con especialidad en Microbiología Aplicada, Universidad Autónoma de Nuevo León, México.

Guo, H., Zhang, X., Song, J., Li, H., & Zou, W. (2022). Green sulfidated iron oxide nanocomposites for efficient removal of Malachite Green and Rhodamine B from aqueous solution. *Water Science and Technology 85*(4), 1202-1217. https://doi.org/10.2166/wst.2022.029

Ibitoye, E. B., Lokman, I. H., Hezmee, M. N. M., Goh, Y. M., Zuki, A. B. Z., & Jimoh, A. A. (2018). Extraction and physicochemical characterization of chitin and chitosan isolated from house cricket. *Biomedical Materials 13*(2), 1-12. https://doi.org/10.1088/1748-605X/aa9dde

Khademian, E., Salehi, E., Sanaeepur, H., Galiano, F., & Figoli, A. (2020). A systematic review on carbohydrate biopolymers for adsorptive remediation of copper ions from aqueous environments-part A: Classification and modification strategies. *Science of The Total Environment 738*, 139829. https://doi.org/10.1016/j.scitotenv.2020.139829

Kuczajowska-Zadrozna, M., Filipkowska, U., & Jóźwiak, T. (2020). Adsorption of Cu (II) and Cd (II) from aqueous solutions by chitosan immobilized in alginate beads. *Journal of Environmental Chemical Engineering 8*(4), 1-7. https://doi.org/10.1016/j.jece.2020.103878

Kumararaja, P., Manjaiah, K. M., Datta, S. C., Ahammed Shabeer, T. P., & Sarkar, B. (2018). Chitosan-g-poly(acrylic acid)-bentonite composite: a potential immobilizing agent of heavy metals in soil. *Cellulose 25*, 3985-3999. https://doi.org/10.1007/s10570-018-1828-x

Lawrie, G., Keen, I., Drew, B., Chandler-Temple, A., Rintoul, L., Fredericks, P., & Grøndahl, L. (2007). Interactions between Alginate and Chitosan Biopolymers Characterized Using FTIR and XPS. *Biomacromolecules 8*(8), 2533-2541. https://doi.org/10.1021/bm070014y

Liu, X., Jiang, Y., He, D., Fang, X., Xu, J., Lee, Y. W., Keller, N. P., & Shi, J. (2020). Copper Tolerance Mediated by FgAceA and FgCrpA in *Fusarium graminearum*. *Frontiers in Microbiology 11*(June), 1-12. https://doi.org/10.3389/fmicb.2020.01392

Liu, Y., Liao, T., He, Z., Li, T., Wang, H., Hu, X., Guo, Y., & He, Y. (2013). Biosorption of copper(II) from aqueous solution by *Bacillus subtilis* cells immobilized into chitosan beads. *Transactions of Nonferrous Metals Society of China 23*(6), 1804-1814. https://doi.org/10.1016/S1003-6326(13)62664-3

Londoño Franco, L. F., Londoño Muñoz, P. T., & Muñoz Garcia, F. G. (2016). Los riesgos de los metales pesados en la salud humana y animal. *Biotecnología en el Sector Agropecuario y Agroindustrial 14*(2), 145-153. https://doi.org/10.18684/BSAA(14)145-153

McCuen, R. H., Knight, Z., & Cutter, A. G. (2006). Evaluation of the Nash-Sutcliffe Efficiency Index. *Journal of Hydrologic Engineering 11*(6), 597-602. https://doi.org/10.1061/(ASCE)1084-0699(2006)11:6(597)

Mokale, V., Jitendra, N., Yogesh, S., & Gokul, K. (2014). Chitosan reinforced alginate controlled release beads of losartan potassium: Design, formulation and in vitro evaluation. *Journal of Pharmaceutical Investigation 44*(4), 243-252. https://doi.org/10.1007/s40005-014-0122-7

Nastaj, J., Przewłocka, A., & Rajkowska-Myśliwiec, M. (2016). Biosorption of Ni(II), Pb(II) and Zn(II) on calcium alginate beads: equilibrium, kinetic and mechanism studies. *Polish Journal of Chemical Technology 18*(3), 81-87. https://doi.org/10.1515/pjct-2016-0052

National Institutes of Health. (2019). *Cobre*. https://ods.od.nih.gov/factsheets/Copper-DatosEnEspanol/

Nouha, K., Kumar, R. S., & Tyagi, R. D. (2016). Heavy metals removal from wastewater using extracellular polymeric substances produced by *Cloacibacterium normanense* in wastewater sludge supplemented with crude glycerol and study of extracellular polymeric substances extraction by different methods. *Bioresource Technology 212*, 120-129. https://doi.org/10.1016/j.biortech.2016.04.021

Nurak, G., Siripor, A., Morales Futulan, C., Tsai, W.-C., Kan, C.-C., & Wan, M.-W. (2012). The Study of Copper Adsorption from Aqueous Solution Using Crosslinked Chitosan Immobilized on Bentonite. *Journal of Applied Polymer Science*, 2-11. https://doi.org/10.1002/app

Papageorgiou, S. K., Kouvelos, E. P., Favvas, E. P., Sapalidis, A. A., Romanos, G. E., & Katsaros, F. K. (2010). Metal-carboxylate interactions in metal-alginate complexes studied with FTIR spectroscopy. *Carbohydrate Research 345*(4), 469-473. https://doi.org/10.1016/j.carres.2009.12.010

Parameswari, E., Ilakiya, T., Davamani, V., Kalaiselvi, P., & Sebastian, S. P. (2021). *Metallothioneins: Diverse Protein Family to Bind Metallic Ions* (M. K. Nazal & H. Zhao (eds.); p. Ch. 9). IntechOpen. https://doi.org/10.5772/intechopen.97658

Pedroso-Santana, S., & Fleitas-Salazar, N. (2020). Ionotropic gelation method in the synthesis of nanoparticles/microparticles for biomedical purposes. *Polymer International 69*(5), 443-447. https://doi.org/10.1002/pi.5970

Pinzón-Bedoya, M. L., & Villamizar, L. E. V. (2009). Modelamiento de la cinética de bioadsorción de Cr (iii) usando cáscara de naranja. *DYNA (Colombia) 76*(160), 95-106. https://www.redalyc.org/articulo.oa?id=49612068033

Rahman, M. S., & Sathasivam, K. V. (2015). Heavy Metal Adsorption onto *Kappaphycus sp*. from Aqueous Solutions: The Use of Error Functions for Validation of Isotherm and Kinetics Models. *BioMed Research International 2015*, 1-13. https://doi.org/10.1155/2015/126298

Rodríguez Heredia, D. (2017). Intoxicación ocupacional por metales pesados. *Medisan 21*(12), 3372-3385. http://scielo.sld.cu/scielo.php?script=sci_arttext&pid=S1029-30192017001200012

Romero-Lázaro, E. M., Ramos-Pérez, D., Martín Romero, F., & Sedov, S. (2019). Indicadores indirectos de contaminación residual en suelos y sedimentos de la cuenca del río Sonora, México. *Revista Internacional de Contaminación Ambiental 35*(2), 371-386. https://doi.org/10.20937/RICA.2019.35.02.09

Sahoo, T. R., & Prelot, B. (2020). Adsorption processes for the removal of contaminants from wastewater: The perspective role of nanomaterials and nanotechnology. In *Nanomaterials for the Detection and Removal of Wastewater Pollutants*. Elsevier Inc. https://doi.org/10.1016/B978-0-12-818489-9.00007-4

Saif, F. A., Yaseen, S. A., Alameen, A. S., Mane, S. B., & Undre, P. B. (2021). Identification and characterization of *Aspergillus* species of fruit rot fungi using microscopy, FT-IR, Raman and UV-Vis spectroscopy. *Spectrochimica Acta - Part A: Molecular and Biomolecular Spectroscopy 246*, 1-10. https://doi.org/10.1016/j.saa.2020.119010

Samuel, J., Pulimi, M., Paul, M. L., Maurya, A., Chandrasekaran, N., & Mukherjee, A. (2013). Batch and continuous flow studies of adsorptive removal of Cr(VI) by adapted

bacterial consortia immobilized in alginate beads. *Bioresource Technology 128*, 423-430. https://doi.org/10.1016/j.biortech.2012.10.116

Sánchez-Duarte, R. G., Martínez-Macías, M. del R., Correa-Murrieta, M. A., Saldívar-Cabrales, J., Sánchez-Machado, D. I., & López-Cervantes, J. (2017). Síntesis de hidrogeles de quitosano a partir de cáscara de camarón para ensayos de adsorción de cobre. *Revista Internacional de Contaminacion Ambiental 33*(Special Issue 1), 93-98. https://doi.org/10.20937/RICA.2017.33.esp02.09

SEMARNAT. (1994). Norma Oficial Mexicana NOM-127-SSA1-1994, Salud ambiental, agua para uso y consumo humano-Límites permisibles de calidad y tratamientos a que debe someterse el agua para su potabilización. https://www.dof.gob.mx/nota_detalle.php?codigo=2063863&fecha=31/12/1969#gsc.tab=0

SEMARNAT. (1996). Norma Oficial Mexicana NOM-001-SEMARNAT- 1996, que establece los límites máximos permisibles de contaminantes en las descargas de aguas residuales en aguas y bienes nacionales. En *Diario Oficial de la Federación*.

Stern, B. R. (2010). Essentiality and toxicity in copper health risk assessment: Overview, update and regulatory considerations. *Journal of Toxicology and Environmental Health - Part A: Current Issues 73*(2-3), 114-127. https://doi.org/10.1080/15287390903337100

Suteu, D., Zaharia, C., & Badeanu, M. (2016). Kinetic modeling of dye sorption from aqueous solutions onto apple seed powder. *Cellulose Chemistry and Technology 50*(9-10), 1085-1091.

Tan, W. S., & Ting, A. S. Y. (2012). Efficacy and reusability of alginate-immobilized live and heat-inactivated *Trichoderma asperellum* cells for Cu (II) removal from aqueous solution. *Bioresource Technology 123*, 290-295. https://doi.org/10.1016/j.biortech.2012.07.082

Tejeda-Tovar, C., Villabona-Ortíz, A., Ortega-Toro, R., López-Génes, J., & Negrete-Palacio, A. (2021). Elimination of Cadmium (II) in aqueaous solution using corn cob (*Zea mays*) in batch system: adsorption kinetics and equilibrium. *Revista Mexicana de Ingeniería Química 20*(1), 1059-1077.

Torres-Caban, R., Vega-Olivencia, C. A., Alamo-Nole, L., Morales-Irizarry, D., Roman-Velazquez, F., & Mina-Camilde, N. (2019). Removal of copper from water by adsorption with Calcium-Alginate/Spent-Coffee-Grounds composite beads. *Materials 12*(3). https://doi.org/10.3390/ma12030395

Torres, M. L., Corizo, A. M., Oberti, T. G., & Fernández, J. M. (2016). Characterization of commercial and algae (Undaria pinnatifida) extracted sodium alginate for future application in bone tissue engineering.

Upadhyay, U., Sreedhar, I., Singh, S. A., Patel, C. M., & Anitha, K. L. (2021). Recent advances in heavy metal removal by chitosan based adsorbents. *Carbohydrate Polymers 251*, 1-29. https://doi.org/10.1016/j.carbpol.2020.117000

Varnam, A. H., & Evans, M. G. (2000). *Environmental Microbiology* (M. P. Ltd (ed.)).

Velkova, Z., Kirova, G., Stoytcheva, M., Kostadinova, S., Todorova, K., & Gochev, V. (2018). Immobilized microbial biosorbents for heavy metals removal. *Engineering in Life Sciences 18*(12), 871-881. https://doi.org/10.1002/elsc.201800017

Vendruscolo, F., da Rocha Ferreira, G. L., & Antoniosi Filho, N. R. (2017). Biosorption of hexavalent chromium by microorganisms. *International Biodeterioration and Biodegradation*. https://doi.org/10.1016/j.ibiod.2016.10.008

Vijayaraghavan, K., & Yun, Y. S. (2008). Bacterial biosorbents and biosorption. *Biotechnology Advances 26*(3), 266-291. https://doi.org/10.1016/j.biotechadv.2008.02.002

Wang, J., & Guo, X. (2020). Adsorption kinetic models: Physical meanings, applications, and solving methods. *Journal of Hazardous Materials 390*, 1-18. https://doi.org/10.1016/j.jhazmat.2020.122156

Xu, J., Song, X. C., Zhang, Q., Pan, H., Liang, Y., Fan, X. W., & Li, Y. Z. (2011). Characterization of metal removal of immobilized *Bacillus* strain CR-7 biomass from aqueous solutions. *Journal of Hazardous Materials 187*(1-3), 450-458. https://doi.org/10.1016/j.jhazmat.2011.01.047

Yu, K., Ho, J., McCandlish, E., Buckley, B., Patel, R., Li, Z., & Shapley, N. C. (2013). Copper ion adsorption by chitosan nanoparticles and alginate microparticles for water purification applications. *Colloids and Surfaces A: Physicochemical and Engineering Aspects 425*, 31-41. https://doi.org/10.1016/j.colsurfa.2012.12.043

Zazzali, I., Aguirre Calvo, T. R., Pizones Ruíz-Henestrosa, V. M., Santagapita, P. R., & Perullini, M. (2019). Effects of pH, extrusion tip size and storage protocol on the structural properties of Ca(II)-alginate beads. *Carbohydrate Polymers 206*(July 2018), 749-756. https://doi.org/10.1016/j.carbpol.2018.11.051